

X-ray spectral analysis of optically faint sources in the *Chandra* Deep Fields

Francesca Civano^{1,2*}, Andrea Comastri^{2*}, Marcella Brusa^{3,2*}

¹*Dipartimento di Astronomia, Università di Bologna, via Ranzani 1, I-40127 Bologna, Italy*

²*INAF – Osservatorio Astronomico di Bologna, via Ranzani 1, I-40127 Bologna, Italy*

³*Max Planck Institut für Extraterrestrische Physik, Giessenbachstrasse 1, D-85748 Garching, Germany*

Accepted 2005

ABSTRACT

We present the results of a detailed spectral analysis of optically faint hard X-ray sources in the *Chandra* deep fields selected on the basis of their high X-ray to optical flux ratio (X/O). The stacked spectra of high X/O sources in both *Chandra* deep fields, fitted with a single power-law model, are much harder than the spectrum of the X-ray background (XRB). The average slope is also insensitive to the 2–8 keV flux, being approximately constant around $\Gamma \simeq 1$ over more than two decades, strongly indicating that high X/O sources represent the most obscured component of the XRB. For about half of the sample, a redshift estimate (in most of the cases a photometric redshift) is available from the literature. Individual fits of a few of the brightest objects and of stacked spectra in different redshift bins imply column densities in the range $10^{22-23.5} \text{ cm}^{-2}$. A trend of increasing absorption towards higher redshifts is suggested.

Key words: Surveys – Galaxies: active — X-ray: galaxies – X-rays: general – X-rays: diffuse background

1 INTRODUCTION

Thanks to the deep surveys carried out by *Chandra* and XMM–Newton X-ray satellites, the hard (2–8 keV) X-ray sky is now probed down to a flux limit of about $2 \times 10^{-16} \text{ erg cm}^{-2} \text{ s}^{-1}$ where a fraction as large as 80% of the diffuse XRB is resolved into discrete sources (Mushotzky et al. 2000; Hasinger et al. 2001; Rosati et al. 2002; Alexander et al. 2003).

The outcomes of these surveys confirm the basic predictions of AGN synthesis models: the integrated emission of obscured and unobscured AGN folded with an appropriate evolving luminosity function is responsible of the spectral intensity of the hard XRB (Setti & Woltjer 1989; Comastri et al. 1995; Gilli, Salvati & Hasinger 2001). The expected source counts at both hard and soft X-ray energies are also in agreement with the observed logN–logS (Moretti et al. 2003); moreover, the observed average spectrum of the resolved source population almost exactly matches that of the XRB ($\langle \Gamma \rangle \sim 1.4$; Tozzi et al. 2001; Nandra et al. 2004).

Massive campaigns of optical and near-infrared follow-up observations have reached a high completeness level. If, on the one hand, the observed redshift and absorption distribution are only poorly reproduced by AGN synthesis models for the X-ray background, calling for some revisions of the underlying assumptions,

on the other hand it has been pointed out that the observed redshift distribution could be significantly biased against the optically faintest, presumably obscured high redshift objects (Fiore et al. 2003; Treister et al. 2004). A solid estimate of the high luminosity, high-redshift tail of the AGN luminosity function is a key parameter to understand the evolution of accretion powered sources and their present day quiescent massive black holes which appear to be ubiquitous in local galaxies (see, e.g., Ferrarese & Merritt 2000).

It is well known that the X-ray to optical flux ratio (hereinafter X/O, see next section for a definition) could provide a first, rough indication of the source classification (Maccacaro et al. 1988). The majority of X-ray selected, relatively unobscured quasars and Seyfert galaxies are characterized by $-1 < X/O < 1$, while obscured AGN have, on average, higher X-ray to optical flux ratios. Combining the X-ray and optical photometry of several hundreds of sources detected by both *Chandra* and XMM–Newton over a broad range of fluxes, about 20% of hard X-ray selected objects are characterized by high X/O values (> 1) and their fraction does not depend upon the X-ray flux (Brusa 2004). The optical magnitudes of high X/O sources detected at relatively bright X-ray fluxes are of the order of $R \simeq 24$ and thus accessible to spectroscopy with large telescopes. Well defined samples of high X/O sources detected in the HELLAS2XMM surveys at X-ray fluxes brighter than $\sim 10^{-14} \text{ erg cm}^{-2} \text{ s}^{-1}$ have been the subject of intensive FORS/VLT optical spectroscopy (Fiore et al. 2003) and near-infrared K_s ISAAC/VLT photometry (Mignoli et al. 2004). The

* E-mail: francesca.civano@bo.astro.it (FC); andrea.comastri@bo.astro.it (AC); marcella@mpe.mpg.de (MB)

results clearly indicate that the majority of the targets are high-redshift ($z > 1$), luminous, X-ray obscured AGN (Perola et al. 2004). The X/O selection is thus highly efficient in sampling high redshift obscured quasars (see also Brusa et al. 2004).

Independent arguments suggesting obscured accretion at high redshifts as a likely explanation of high X/O ratios have been discussed by Comastri, Brusa and Mignoli (2003). Moving the Spectral Energy Distribution (SED) of an X-ray absorbed AGN to progressively higher redshifts the K-corrections in the optical and X-ray band work in the opposite direction. The ratio between the optical to X-ray optical depth, in the observer frame, scales roughly as $(1+z)^{3.6}$, because dust extinction increases in the UV while X-ray absorption strongly decreases going toward high energies. The net result is that in the presence of an absorbing screen the observed optical flux of a high- z AGN can be strongly reduced, and the observed magnitudes are mainly due to starlight in the host galaxies. Conversely, the hard X-ray flux is much less affected. The observed high values of the X/O are therefore at least qualitatively consistent with those expected by a population of high redshift, absorbed AGN with X-ray column densities in the range $N_H = 10^{22} - 10^{24} \text{ cm}^{-2}$.

At the limits of deep *Chandra* surveys, high X/O sources are characterized by extremely faint optical magnitudes and spectroscopic identification is not feasible even with the largest telescopes. In this framework a detailed investigation of their X-ray properties may provide useful information on the nature of this important component of the X-ray source population. We present and discuss in the following the results of detailed X-ray spectral analysis, including the search for iron $K\alpha$ lines, combined with the available multiwavelength information for a large sample of high X/O sources in the *Chandra* Deep Field North (Alexander et al. 2003) and the *Chandra* Deep Field South (Giacconi et al. 2002; hereinafter CDFN and CDFS). A cosmological model with $H_0 = 70 \text{ km s}^{-1} \text{ Mpc}^{-1}$, $\Omega_m = 0.3$ and $\Omega_\Lambda = 0.7$ is assumed.

2 SAMPLE SELECTION

We have selected 127 hard X-ray sources in the *Chandra* Deep Fields (63 in the CDFN and 64 in the CDFS) with an X-ray to optical flux ratio $\log(f_X/f_R) > 1$ defined as:

$$X/O = \log \frac{f_X}{f_R} = \log f_X + C + \frac{R}{2.5} \quad (1)$$

where f_X is the X-ray flux ($\text{erg cm}^{-2} \text{ s}^{-1}$) in a given energy range, f_R is the R-band flux computed by converting the R-band magnitudes into monochromatic fluxes (at $\lambda=6500\text{\AA}$) and then multiplying them by the width of the R filter (Zombeck 1990), C is a constant which depends on the specific filter used in the optical observations. In order to be consistent with the published optical catalogues we used $C=5.5$ for the CDFN and $C=5.71$ for the CDFS. The hard band (2–8 keV) fluxes and the basic X-ray source properties (positions, counts, exposure times) have been compiled from the Alexander et al. (2003) X-ray source catalogue for CDFN and CDFS. The R-band magnitudes along with optical identification and classification (when available) have been retrieved from Barger et al. (2003) for the CDFN, Giacconi et al. (2002), Szokoly et al. (2004) and Zheng et al. (2004) for the CDFS. Figure 1 shows the R-band magnitude versus the 2–8 keV flux for the 127 high X/O sources discussed in this work.

For each source we report in Table 1 and 2 the X-ray identification number (col. 1), the X-ray coordinates (col. 2 and 3), the

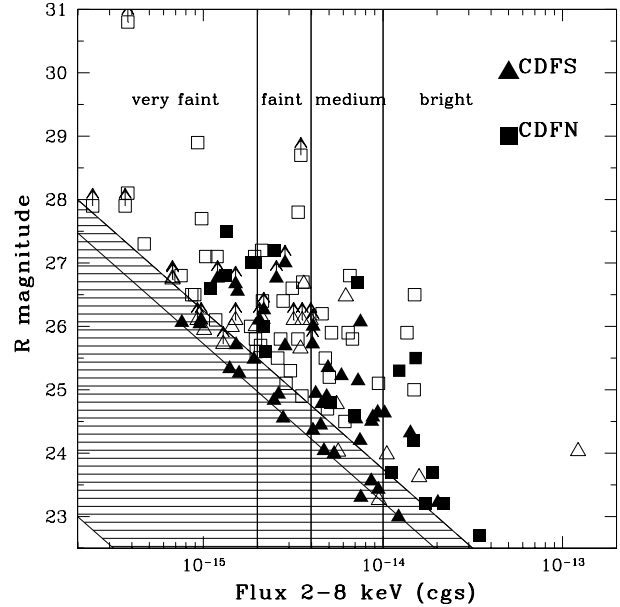


Figure 1. The R-band magnitude vs. the 2–8 keV flux for the 127 high X/O sources selected from the CDFN (squares) and CDFS (triangles) samples. Filled symbols are objects with redshift identification. The dashed area represents the locus occupied by known AGN (e.g. quasars, Seyferts, emission-line galaxies) along the correlation $\log(X/O)=0\pm1$. Two upper boundaries at $\log(X/O)=1$ are reported as we used two different constants for the CDFN and the CDFS (see Sect. 2 for details). The vertical lines are the boundaries of the 4 flux bins discussed in Section 4.1.

hard X-ray flux (col. 4), the optical R-band magnitude (col. 5), the magnitude reference for CDFS (col. 6) and the X/O from equation 1 (col. 7 and 6, respectively). Sources undetected in the R band are reported as lower limits in Tables 1–2 and in these cases the X/O ratio has to be considered a lower limit. All the high X/O objects represent $\sim 23\%$ of the hard X-ray sources revealed in both deep fields.

3 DATA REDUCTION

The CDFS 1 Megasecond dataset is the result of the co-addition of 11 individual *Chandra* ACIS-I exposures whose aimpoints are at a few arcsec from each other. The total area covered is $\sim 392 \text{ arcmin}^2$; this field was selected in a patch of the southern sky (nominal aim point $\alpha_{2000} = 03^h 32^m 28^s.0$ e $\delta_{2000} = -27^\circ 48' 30''$) characterized by a very low Galactic neutral hydrogen column density ($8 \times 10^{19} \text{ cm}^{-2}$) and by the lack of bright stars (Rosati et al. 2002).

The CDFN has been observed by about 2 Megaseconds over a period of 27 month, and is the result of the co-addition of 20 individual *Chandra* ACIS-I exposures centered (nominal aim point $\alpha_{2000} = 12^h 36^m 49^s.4$ $\delta_{2000} = 62^\circ 12' 58''$) close to the Hubble Deep Field North (HDF-N, Williams et al. 1996), the most studied region of the sky with a low Galactic neutral hydrogen column density ($1.6 \times 10^{20} \text{ cm}^{-2}$, Stark et al. 1992). Due to the different pointings, required to keep the HDF-N near the aim point and the *Chandra* roll angle constraints, the area covered is 447.8 arcmin^2 .

The X-ray data have been retrieved from the public archive and processed with standard tools making use of the calibrations

Table 1. Properties of high X/O sources in the CDFS.

XID	RA	DEC	f_X^a	R	Ref. ^b	X/O	z	z type ^c
3	3:33:05.85	-27:46:50.2	3.18	>26.10	G	>1.65	...	+
8	3:33:01.44	-27:41:42.0	9.40	23.43	S	1.06	0.99	phot (0.9)
20a	3:32:44.47	-27:49:40.2	5.34	23.99	S	1.03	1.016	spec
23	3:32:41.85	-27:43:59.9	2.62	24.93	S	1.10	0.73	phot (0.5)
25	3:32:40.84	-27:55:46.6	9.34	24.64	S	1.54	2.26	phot (0.5)
26	3:32:39.73	-27:46:11.2	2.78	24.55	S	0.97 [†]	1.624	phot (0.5)
27	3:32:39.68	-27:48:50.7	7.06	24.54	S	1.37	3.064	spec
31	3:32:37.77	-27:52:12.4	8.78	24.57	S	1.48	1.603	spec
35	3:32:34.37	-27:39:13.1	14.2	24.32	S	1.59	1.51	spec
45	3:32:25.68	-27:43:05.8	4.94	25.35	S	1.54	2.291	spec
48	3:32:24.84	-27:56:00.0	4.86	24.89	G	1.35	0.841	phot ^d
51a	3:32:17.18	-27:52:20.9	20.2	23.22	S	1.30	1.097	spec
54	3:32:14.57	-27:54:21.6	2.85	25.69	S	1.44	2.561	spec
57	3:32:12.95	-27:52:36.7	4.69	24.04	S	1.00	2.562	spec
58	3:32:11.77	-27:46:28.2	1.96	26.00	S	1.40	...	*
59	3:32:11.41	-27:52:13.5	6.21	26.47	S	2.09	...	++
61	3:32:10.50	-27:43:09.0	10.5	23.98	S	1.32	...	*
64	3:32:08.00	-27:46:57.2	5.52	24.77	S	1.36	...	+
65	3:32:03.90	-27:53:28.9	2.17	>26.26	S	>1.55	1.10	phot (0.5)
67	3:32:02.46	-27:46:00.3	8.61	23.56	S	1.07	1.616	spec
69a	3:32:01.43	-27:41:38.6	5.63	24.02	S	1.07	...	+
70a	3:32:01.42	-27:46:47.1	15.9	23.62	S	1.36	...	+
72a	3:31:58.29	-27:50:41.6	7.48	26.07	S	2.01	1.99	phot (0.5)
76	3:31:52.50	-27:50:17.5	8.64	24.50	S	1.45	2.394	spec
79	3:32:38.03	-27:46:26.2	1.55	26.55	S	1.52	1.91	phot (0.5)
81	3:32:25.96	-27:45:14.3	0.95	26.04	S	1.11	2.59	phot (0.5)
82a	3:32:14.87	-27:51:03.8	1.51	>26.1	S	>1.33	...	*
99	3:32:05.17	-27:53:54.7	5.87	25.22	S	1.57	0.79	phot (0.5)
108a	3:32:05.77	-27:44:46.6	1.01	25.94	S	1.09	...	*
112	3:31:51.98	-27:53:26.7	2.47	24.83	S	1.03	2.942	spec
133	3:32:02.52	-27:44:29.8	0.67	>26.74	G	>1.23	...	++
145	3:32:22.54	-27:46:03.9	4.56	24.78	S	1.28	1.50	phot (0.5)
146	3:32:47.05	-27:53:33.3	2.55	>26.76	G	>1.82	2.67	phot (0.5)
147	3:32:46.35	-27:46:31.9	7.26	25.14	S	1.63	0.99	phot (0.5)
148	3:32:35.23	-27:53:17.8	2.85	>27	S	>1.96	1.74	phot (0.5)
153	3:32:18.34	-27:50:55.2	7.45	24.20	S	1.26	1.536	spec
159	3:32:50.23	-27:52:51.7	7.53	23.30	S	0.90 [†]	3.3	phot (0.5)
179	3:31:49.49	-27:50:34.0	0.97	>26.10	G	>1.14	2.73	phot (0.5)
201a	3:32:39.06	-27:44:39.1	2.14	26.11	S	1.48	...	*
205a	3:32:17.11	-27:41:36.6	1.44	25.99	S	1.26	...	++
207a	3:32:07.96	-27:37:35.1	122.0	24.03	S	2.41	...	+
209	3:31:47.30	-27:53:13.3	10.2	24.63	S	1.57	1.32	phot (0.5)
213a	3:32:00.56	-27:53:53.0	3.47	25.65	S	1.51	...	++
219	3:31:50.43	-27:51:51.8	3.96	>26.10	G	>1.75	...	*
227	3:32:05.35	-27:46:44.1	3.62	26.67	S	1.94	...	*
243	3:32:08.39	-27:40:47.0	4.05	>25.72	G	>1.61	2.50 ^e	phot (0.3)
253	3:32:20.07	-27:44:47.0	4.22	24.94	S	1.31	1.89	spec
256	3:32:43.05	-27:48:45.0	4.07	24.36	S	1.06	1.53	phot (0.5)
259	3:32:06.13	-27:49:27.7	4.50	24.44	S	1.14	1.76	phot (0.5)
261	3:31:57.03	-27:51:08.6	3.55	>26.10	G	>1.70	...	**
263b	3:32:18.89	-27:51:35.4	1.40	25.33	S	0.99 [†]	3.66	spec
265	3:32:33.27	-27:42:36.1	4.08	>26.00	G	>1.72	1.16	phot (0.5)
501	3:33:10.18	-27:48:41.8	12.2	22.99	S	0.99 [†]	0.81	phot (0.6)
503	3:33:07.61	-27:51:26.6	9.48	23.26	S	0.99 [†]	...	+
505a	3:33:04.83	-27:47:31.9	1.91	25.48	S	1.18	0.981	phot ^d
506	3:33:02.97	-27:51:46.4	0.93	>26.10	G	>1.12	...	*
508	3:32:51.64	-27:52:12.8	1.20	>26.76	G	>1.49	2.5	phot (0.5)
513a	3:32:34.03	-27:48:59.9	0.76	26.06	S	1.01	3.53	phot (0.5)
515	3:32:32.17	-27:46:51.4	1.51	>26.67	G	>1.56	2.19	phot (0.5)
518	3:32:26.75	-27:46:04.3	0.67	>26.76	G	>1.21	...	++
524	3:32:19.96	-27:42:43.2	1.29	>25.72	G	>1.11	...	*
533	3:32:13.90	-27:56:00.1	2.05	>26.10	G	>1.46	0.54	phot (0.5)
595	3:32:15.75	-27:39:53.8	1.52	25.71	S	1.18	0.36	phot (0.5)
606a	3:32:24.97	-27:50:08.2	1.58	25.26	S	1.01	1.037	spec

^a In units of 10^{-15} erg cm⁻² s⁻¹. ^b G = Giacconi et al. 2002, S = Szokoly et al. 2004. ^c The photo-z quality flag (QF) from Zheng et al. (2004) is reported in brackets; QF=0.3 means that the redshift is from the BPZ code; QF=0.5 means that two independent codes (BPZ and HyperZ) return consistent values; QF=0.6 means that HyperZ code returns the same value of COMBO-17 catalogue; QF=0.9 means that the value returned by BPZ and HyperZ is confirmed in the COMBO-17 catalogue. ^d Photometric redshift from COMBO-17 survey catalogue (Wolf et al. 2004). ^e Although QF=0.3, the detection of a K α line (Gilli, private communication) at the best-fit photo-z makes us confident on this value. [†] The 5 sources with X/O slightly lower than 1 would have X/O > 1 if the X-ray flux quoted in Giacconi et al. (2001) is considered. + Sources with QF \leq 0.4 in Zheng et al. (2004). ++ QF=0.5 but with a large error on redshift estimate ($\Delta z \geq 1.0$). * The optical counterpart presented in Zheng et al. (2004) lies at > 2'' from the Alexander et al. (2003) position. ** Source 261 is not present in Zheng et al. (2004).

Table 2. Properties of high X/O sources in the CDFN.

XID	RA	DEC	f_X^a	R	X/O	z	z type ^b
7	12:35:21.71	+62:15:01.6	2.11	27.2	1.704
9	12:35:24.92	+62:15:24.8	4.77	25.5	1.378
10	12:35:28.77	+62:14:27.8	4.58	26.2	1.640
12	12:35:29.45	+62:18:22.8	3.36	25.8	1.346
28	12:35:46.07	+62:15:59.9	2.48	27.2	1.774	1.93	phot
29	12:35:46.25	+62:17:29.8	1.93	27.1	1.625
36	12:35:50.42	+62:18:08.6	12.3	25.3	1.71	0.52	K α
38	12:35:51.75	+62:17:57.1	15.0	26.5	2.276
42	12:35:54.11	+62:20:12.3	0.86	26.5	1.035
48	12:35:56.14	+62:12:19.2	18.8	23.7	1.25	1.13	K α
71	12:36:05.62	+62:06:54.0	1.95	25.8	1.11
73	12:36:05.83	+62:08:38.0	2.78	26.4	1.50
91	12:36:11.40	+62:21:49.9	9.44	25.1	1.51
98	12:36:13.02	+62:12:24.1	1.97	25.6	1.03
92	12:36:11.80	+62:10:14.5	2.69	25.8	1.24
98	12:36:13.02	+62:12:24.1	1.97	25.6	1.03
100	12:36:14.14	+62:10:17.7	0.93	28.9	2.028
102	12:36:14.45	+62:10:45.0	3.54	24.9	1.00
107	12:36:15.83	+62:15:15.5	1.85	27.0	1.567	2.06	phot
108	12:36:16.03	+62:11:07.7	15.2	25.5	1.88	1.25	phot
129	12:36:21.94	+62:16:03.8	1.32	26.8	1.34	2.26	phot
134	12:36:22.65	+62:10:28.5	2.89	25.1	1.00
140	12:36:23.66	+62:10:08.7	0.47	27.3	1.09
146	12:36:25.33	+62:17:37.7	2.21	25.6	1.084	1.28	phot
151	12:36:27.53	+62:12:18.0	0.24	>27.9	>1.04
154	12:36:28.65	+62:21:39.5	14.9	25	1.673
156	12:36:28.78	+62:11:40.0	0.38	>30.8	>2.39
165	12:36:30.15	+62:26:20.1	11.1	23.7	1.025	1.46	phot
186	12:36:34.71	+62:04:37.9	2.08	25.7	1.098
195	12:36:36.85	+62:22:27.4	2.13	26.4	1.38
196	12:36:36.90	+62:13:20.0	0.38	28.1	1.32
204	12:36:38.94	+62:10:41.5	0.37	>27.9	>1.22
232	12:36:44.95	+62:26:51.0	4.91	24.7	1.07
246	12:36:47.94	+62:10:19.9	1.94	27.0	1.58	2.52	phot
250	12:36:48.28	+62:14:56.2	1.34	27.5	1.62	2.09	phot
253	12:36:48.73	+62:21:53.9	2.59	25.5	1.11
259	12:36:49.66	+62:07:38.3	21.8	23.2	1.11	1.609	spec
290	12:36:56.56	+62:15:13.1	0.75	26.8	1.09
318	12:37:01.76	+62:07:20.8	0.98	27.7	1.57
321	12:37:02.43	+62:19:26.1	3.05	25.3	1.10
334	12:37:04.87	+62:16:01.6	6.40	25.9	1.66
335	12:37:05.12	+62:16:34.8	1.03	27.1	1.35
336	12:37:05.31	+62:24:54.8	3.12	26.6	1.63
350	12:37:07.70	+62:05:34.6	1.83	26	1.16
357	12:37:09.40	+62:22:14.4	6.94	24.6	1.18	1.43	phot
374	12:37:13.84	+62:18:26.2	1.19	27.1	1.41
382	12:37:15.19	+62:02:31.0	6.76	25.8	1.64
390	12:37:16.65	+62:17:33.3	17.3	23.2	1.01	1.146	spec
400	12:37:20.26	+62:07:26.7	0.89	26.5	1.05
406	12:37:22.44	+62:05:36.1	3.37	27.8	2.14
412	12:37:24.00	+62:13:04.3	6.13	24.5	1.08
413	12:37:24.29	+62:13:59.7	5.09	24.8	1.13	0.474	spec
444	12:37:36.85	+62:14:29.2	5.16	25.9	1.57
445	12:37:37.04	+62:18:34.4	3.58	26.7	1.73
452	12:37:39.46	+62:22:39.2	3.49	>28.7	>2.52
456	12:37:41.13	+62:10:47.9	1.09	26.6	1.77	1.60	phot
463	12:37:45.02	+62:07:18.9	7.20	26.7	2.03	2.50	phot
465	12:37:46.78	+62:07:12.6	1.17	26.1	1.00
470	12:37:50.22	+62:13:59.3	2.17	26.0	1.23	0.23	spec
490	12:38:10.56	+62:17:29.6	14.8	24.2	1.35	1.02	phot
495	12:38:22.30	+62:14:16.7	34.4	22.7	1.11	0.986	spec
498	12:38:23.66	+62:09:42.4	5.03	25.2	1.28
497	12:38:23.21	+62:15:18.3	6.54	26.8	2.03
501	12:38:34.29	+62:14:40.9	13.6	25.9	1.99

^a In units of 10^{-15} erg cm $^{-2}$ s $^{-1}$. ^b Redshift type: spectroscopic, photometric or from the K α iron line.

associated with the CIAO¹ software (version 3.0). All the observations of both fields have been registered on the deepest one and have been aligned using `align_evt`².

Since the main aim of the present work concerns the average spectral properties of relatively faint sources, the issue of co-adding spectra obtained from observations performed with different aim points and roll angles has to be treated appropriately. In principle for each pointing and each object the source and background spectra, along with the detector position-dependent response matrix and effective area should be computed and then summed together weighting for the exposure time of each observation (“standard” procedure). In practice, such an approach results to be extremely time consuming. In order to compute, from the total merged event file, all the relevant files needed for the spectral analysis an alternative approach has been devised. This approach is based on two CIAO tools `mkwarf` and `mkrmf`³ developed to extract spectral data from multiple regions either from the same or different observations. More specifically, the spectrum and relative background for a sample of sources are extracted from a stack of regions whose shape and size are function of the off-axis angle. The weighted detector position dependent spectral response and effective area are computed taking into account the shape and area of the extraction regions and the number of counts of each individual region in the stack. In order to test whether these tools could be applied to multiple extraction regions in co-added observations, we proceeded as follows.

We considered several different samples of N sources, randomly distributed over the detector in both the CDFN and CDFS merged event files. The size and shape of extraction regions were chosen according to the number of counts and source off-axis angle in each exposure and tuned to enclose the 90% of the PSF at 6.4 keV. This energy has been chosen since our sources have been selected in the hard band (§2). Several background spectra were extracted from a stack of regions nearby each source and varied in size and shape. The corresponding response RMF and effective area ARF file have been computed from the merged event files making use of `mkwarf` and `mkrmf`. The ancillary response files are corrected for the well known degradation of the ACIS quantum efficiency using the latest version of the ACISABS tool⁴.

In order to check the reliability of our procedure with respect to the standard one, we have computed the average stacked spectrum of 30 X-ray sources in the CDFN and 35 in the CDFS spectroscopically identified as broad-line AGN by Barger et al. (2003) and Szokoly et al. (2004), respectively. The best-fit parameters of a single absorbed power law are: $\Gamma=1.73\pm0.03$, $N_H(z=0)=7\pm1\times10^{20}\text{ cm}^{-2}$ in the CDFN and $\Gamma=1.82\pm0.04$, $N_H(z=0)=4.7\pm1.4\times10^{20}\text{ cm}^{-2}$ in the CDFS, slightly flatter ($\Delta\Gamma\sim0.1-0.2$) than the “canonical” value (e.g. $\Gamma=1.9-2.0$; Nandra & Pounds 1994), but fully consistent with the fact that no reflection component has been included in the spectral fitting. Moreover, in the CDFN our results are in excellent agreement with those reported by Bauer et al. (2002) for a sample of broad-line AGN largely overlapping with ours. Given that the Bauer et al. results have been obtained applying a rather different (IDL based) data reduction procedure (ACIS-Extract), we are confident of the reliability of our method.

4 SPECTRAL ANALYSIS

The stacked spectra have been extracted in the 0.7–7 keV band, to minimize residual calibration uncertainties of the low energy instrumental response, and rebinned to have at least 20 counts per bin. X-ray spectral fitting was performed using XSPEC (version 11.3.0; Arnaud 1996); errors are reported at the 90% confidence level for one interesting parameter ($\Delta\chi^2=2.71$). In all the fits, a “negative” edge ($\tau = -0.17$) at 2.07 keV has been included to take into account calibration uncertainties around the instrumental Iridium edge (Vikhlinin et al. 2005).

4.1 Average spectra

The stacked spectra of the high X/O sources in both the CDFN (about 30000 net counts) and CDFS (about 19500 net counts) were fitted with an absorbed power-law model with absorption fixed at the Galactic value (hereinafter MODEL 1).

The resulting best-fit slopes are $\Gamma(\text{CDFN})=0.77\pm0.02$ and $\Gamma(\text{CDFS})=0.97\pm0.03$. Although the residuals (Fig. 2) indicate a more complex curved shape, these extremely hard spectra strongly suggest that high X/O sources represent the most obscured component of the so far resolved XRB. Even more obscured possibly Compton thick AGN, yet undetected in deep surveys, might be responsible of the XRB at higher energies (Worsley et al. 2004). The measured values are significantly flatter than the average spectrum of the total CDFS sample in the 1–10 keV range ($\langle\Gamma\rangle=1.375\pm0.015$; Rosati et al. 2002) as well as of the average XRB slope ($\Gamma \simeq 1.4$) in the same energy range.

Leaving the absorption free to vary (hereinafter MODEL 2) the quality of the fit improves significantly (Fig. 3). The best-fit slopes and column densities are: $\Gamma=1.34\pm0.04$, $N_H(z=0)=4.1\pm0.3\times10^{21}\text{ cm}^{-2}$ for the CDFN and $\Gamma=1.34\pm0.03$, $N_H(z=0)=2.4\pm0.4\times10^{21}\text{ cm}^{-2}$ for the CDFS. Given that the stacked objects are likely to be distributed over a range of redshifts and that no redshift dependence has been considered, the N_H values have to be considered as lower limits to any absorption component. For the same reason the intrinsic power-law slope might well be steeper, the observed value being the result of a distribution of column densities convolved with redshift.

The accumulated source counts in the stacked spectra are sufficient to further investigate the spectral properties of high X/O sources and, in particular, to search for the progressive hardening of the mean spectral slope towards faint fluxes; this hardening has been clearly established both in the CDFS (Rosati et al. 2002) and CDFN (Alexander et al. 2003) total samples.

The high X/O sources of our sample were divided in four 2–8 keV flux intervals (see Fig. 1). The bin width was optimized to keep the total number of counts in each bin adequate to perform spectral analysis. The flux intervals were defined as follows: bright (A, $> 10^{-14}\text{ erg cm}^{-2}\text{ s}^{-1}$), medium (B, $4\times10^{-15} - 10^{-14}\text{ erg cm}^{-2}\text{ s}^{-1}$), faint (C, $2\times10^{-15} - 4\times10^{-15}\text{ erg cm}^{-2}\text{ s}^{-1}$) and very faint (D, $< 2\times10^{-15}\text{ erg cm}^{-2}\text{ s}^{-1}$). Stacked spectra in each subsample were extracted following the procedure described in Sect. 3 and fitted with both MODEL 1 and MODEL 2: the best-fit parameters are reported in Table 3, and shown in Figure 4. There is no clear evidence of a spectral flattening as a function of the X-ray flux, with a possible exception for the CDFN sources fitted with MODEL 2. The average spectrum of high X/O sources remains constant with a very hard slope ($\Gamma \lesssim 1$) over about two decades of X-ray flux and definitely flatter than that measured for the entire CDFS and CDFN samples down to comparable limiting fluxes (see

¹ <http://cxc.harvard.edu/ciao/>

² http://cxc.harvard.edu/cal/ASPECT/align_evt/

³ http://asc.harvard.edu/ciao/threads/wresp_multiple_sources/

⁴ http://chandra.ledas.ac.uk/ciao3.0/threads/apply_acisabs/

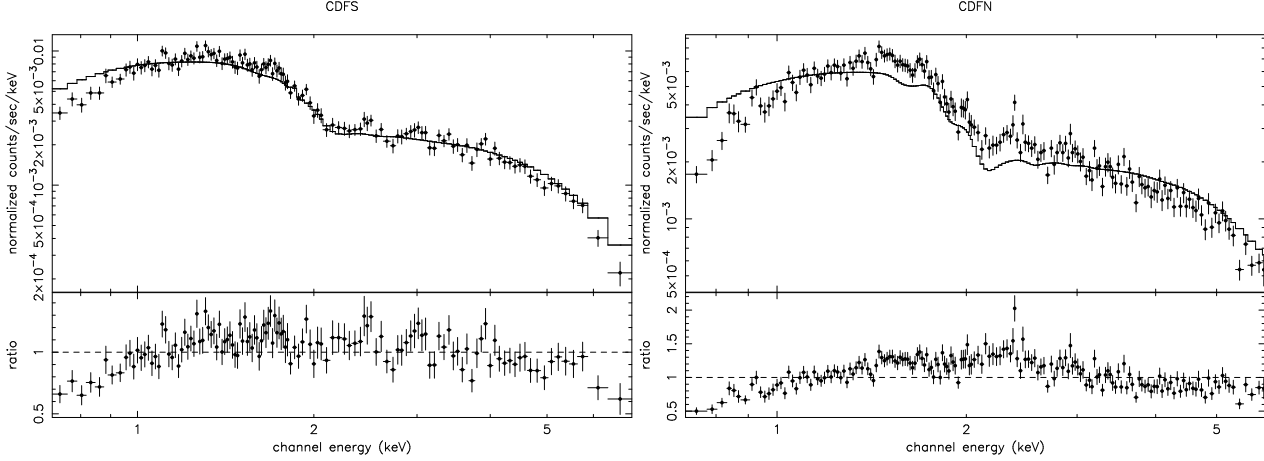


Figure 2. Stacked spectra of all the high X/O sources in CDFS (64 sources) and CDFN (63 sources), fitted in the 0.7-7 keV energy band with a power-law spectrum (MODEL 1). The best-fit spectral slopes are reported in Table 3. The solid line is the best-fit model, while the lower panel shows the data-to-model ratio.

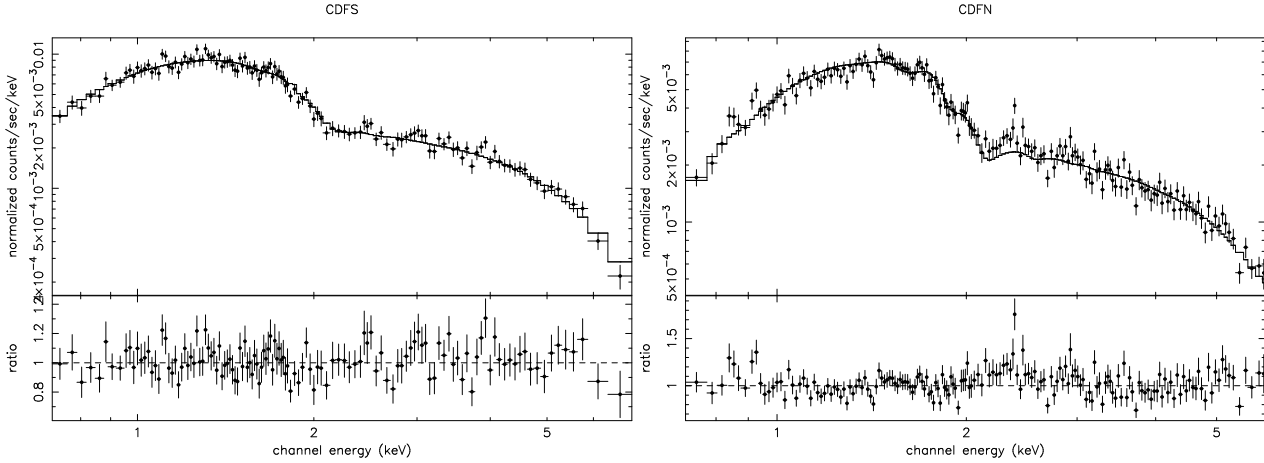


Figure 3. Stacked spectra of all the high X/O sources selected in CDFS (64 sources) and CDFN (63 sources), fitted in the 0.7-7 keV energy band with an absorbed power-law spectrum (MODEL 2). The best-fit column densities and spectral slopes are reported in Table 3. The solid line is the best-fit model, while the lower panel shows the data-to-model ratio.

Fig. 5). The difference is more pronounced ($\Delta\Gamma \sim 0.7$) at fluxes brighter than $\sim 5 \times 10^{-15} \text{ erg cm}^{-2} \text{ s}^{-1}$, which are dominated by unobscured quasars with a soft X-ray spectrum, decreasing to $\Delta\Gamma \sim 0.15$ at fainter fluxes, where the contribution of obscured sources with $X/O < 1$ to the total sample is much higher.

A very flat 2–10 keV spectrum may also be the signature of a strong Compton reflection component and is expected for column densities in the Compton-thick regime ($N_H \gtrsim 2 \times 10^{24} \text{ cm}^{-2}$). Spectral fits performed with a pure reflection spectrum (model `pexrav` in `XSPEC`) do not provide a statistically acceptable description of the data leaving significant residuals at low energy. The most straightforward explanation of the observed flat slope in the stacked spectra is in terms of the superposition of different photoelectric cut-offs due to Compton-thin absorption likely spread over a broad range of redshifts.

4.2 Redshift determination through $K\alpha$ iron line

The residuals of a single power-law fit to the average spectrum of the CDFN bright subsample (A) are highly indicative of the presence of a line-like feature. Given that the iron line at 6.4 keV is

by far the strongest emission feature in the X-ray band, it can be used as a redshift indicator. The 11 sources in subsample A have a counting statistic which is such to allow for individual spectral analysis: spectra were extracted for these sources and fitted with MODEL 2. A clear excess suggesting the presence of an iron-line has been found in 4 of them (XID 36, 48, 259, 390). The $\text{Fe}K\alpha$ line of source 390 has been already extensively discussed by Comastri, Brusa & Civano (2004). A spectroscopic redshift ($z_{\text{spec}} = 1.609$) has been measured by Barger et al. (2003) for source 259; this value is fully consistent with that inferred from the iron $K\alpha$ line ($z_{X\text{-ray}} = 1.60 \pm 0.05$).

The addition of a narrow Gaussian line due to cold iron ($E_{\text{rest}} = 6.4 \text{ keV}$) in MODEL 2 improves the fit by $\Delta\chi^2 \simeq 9$ and $\simeq 15$ for source 36 and 48, respectively. The observed line energy corresponds to an X-ray redshift of $z = 0.52^{+0.03}_{-0.05}$ and $z = 1.13 \pm 0.05$. In figure 6 and 7 the spectra and the confidence contours of redshift versus line intensity are shown. The rest frame equivalent widths are $293 \pm 204 \text{ eV}$ and $400^{+201}_{-195} \text{ eV}$, respectively. Assuming the redshift estimated by the iron line, the inferred column densities are $N_H = 1.20 \pm 0.15 \times 10^{22} \text{ cm}^{-2}$ and $N_H = 3.2 \pm 0.3 \times 10^{23} \text{ cm}^{-2}$, respectively. The absorp-

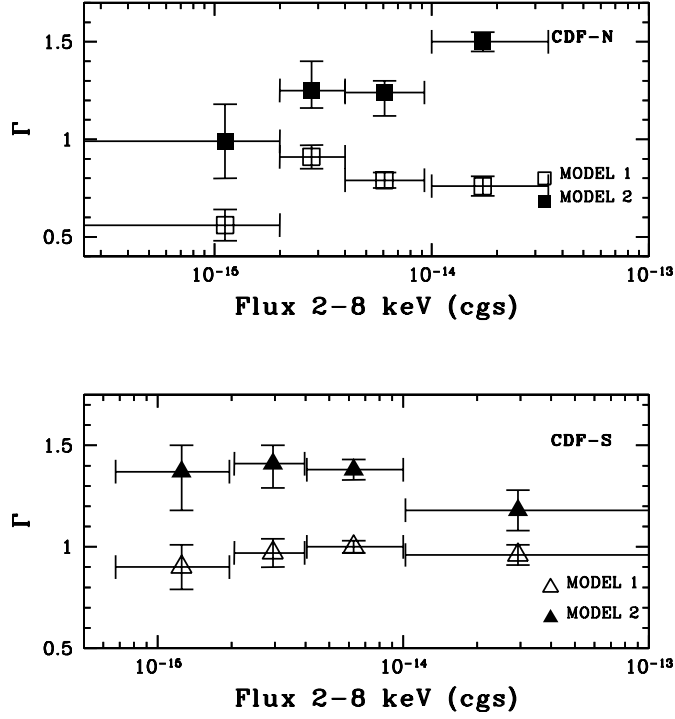


Figure 4. Spectral index Γ vs. hard X-ray flux obtained with MODEL 1 (open symbols) and MODEL 2 (filled symbols) for the 4 subsamples of CDFN (squares, top panel) and CDFS (triangles, bottom panel). The errors on the slope are at the 90% confidence level; the horizontal bars represent the bin width.

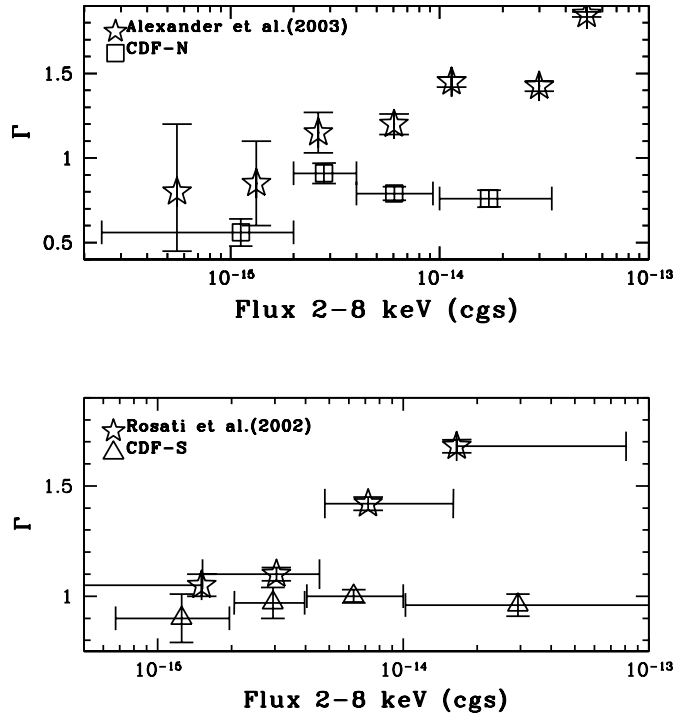


Figure 5. Top panel: Spectral index Γ vs. hard X-ray flux obtained with MODEL 1 for high X/O CDFN subsamples (squares) compared with the values of Γ as obtained from band ratios for the entire CDFN sample (stars, Alexander et al. 2001, 2003). Bottom panel: Spectral index Γ vs hard X-ray flux obtained with MODEL 1 for high X/O CDFS subsamples (triangles) compared with the values obtained for all CDFS hard sample (stars, Rosati et al. 2002)

Table 3. Spectral fit parameters obtained with MODEL 1 and MODEL 2.

	Sample ^a	Model	Γ	$N_H(z=0)^b$	$\chi^2/\text{d.o.f.}$
CDFS	all (64)	MODEL 1	0.97 ± 0.03	Galactic ^c	429.2/261
		MODEL 2	1.34 ± 0.03	0.24 ± 0.04	255.8/260
	A (7)	MODEL 1	0.96 ± 0.05	Galactic	133.6/109
		MODEL 2	1.18 ± 0.1	0.15 ± 0.05	115.9/108
	B (25)	MODEL 1	1.00 ± 0.03	Galactic	368.3/254
		MODEL 2	1.38 ± 0.05	0.25 ± 0.04	259.1/253
	C (14)	MODEL 1	0.97 ± 0.07	Galactic	137.2/125
		MODEL 2	$1.41^{+0.09}_{-0.12}$	$0.27^{+0.09}_{-0.06}$	107.3/124
	D (18)	MODEL 1	0.90 ± 0.11	Galactic	105.9/99
		MODEL 2	$1.37^{+0.13}_{-0.19}$	$0.31^{+0.17}_{-0.11}$	92.3/98
CDFN	all (63)	MODEL 1	0.77 ± 0.02	Galactic ^d	1137.7/374
		MODEL 2	1.34 ± 0.04	0.41 ± 0.03	473.2/373
	A (11)	MODEL 1	0.76 ± 0.05	Galactic	1091.0/257
		MODEL 2	1.50 ± 0.05	0.53 ± 0.03	361.7/256 ^e
	B (13)	MODEL 1	0.79 ± 0.04	Galactic	279.0/168
		MODEL 2	$1.24^{+0.06}_{-0.12}$	0.30 ± 0.05	196.7/167
	C (17)	MODEL 1	0.91 ± 0.06	Galactic	180.2/151
		MODEL 2	$1.25^{+0.15}_{-0.09}$	$0.23^{+0.08}_{-0.04}$	146.0/150
	D (22)	MODEL 1	0.56 ± 0.08	Galactic	133.4/109
		MODEL 2	0.99 ± 0.19	$0.33^{+0.14}_{-0.10}$	113.6/108

^a The number of sources in each bin is reported in brackets. ^b Units of 10^{22} cm^{-2} .

^c $N_H(\text{Gal})(\text{CDFS}) = 8 \times 10^{19} \text{ cm}^{-2}$. ^d $N_H(\text{Gal})(\text{CDFN}) = 1.6 \times 10^{20} \text{ cm}^{-2}$. ^e The quality of the fit is not good due to features around 3 keV (see Sect. 4.2).

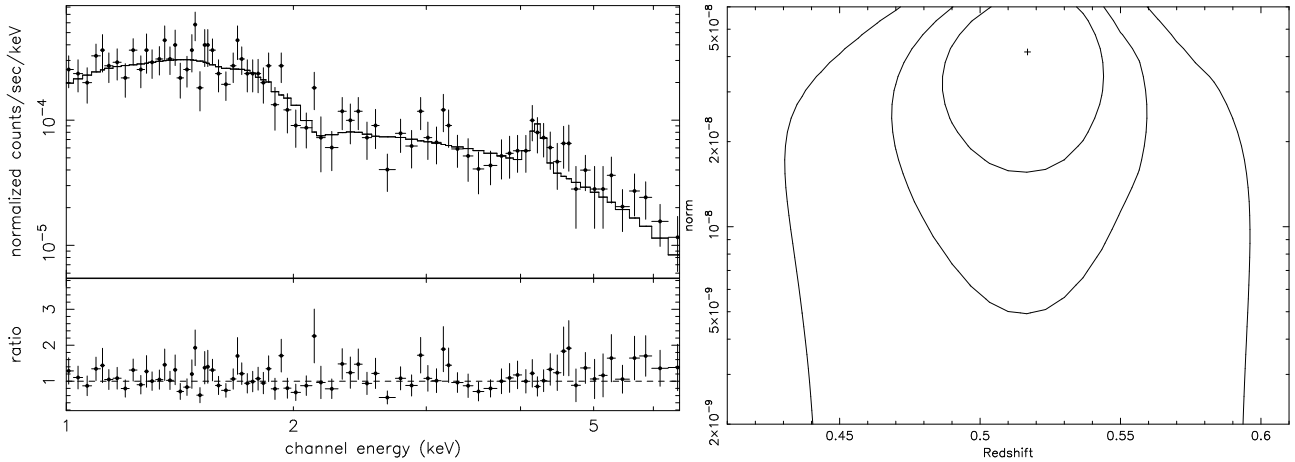


Figure 6. Left panel: the X-ray spectrum of source 36 (CDFN), fitted with an absorbed power-law plus a FeK α line (the best fit column density and spectral slope are $N_H = 1.20 \pm 0.15 \times 10^{22} \text{ cm}^{-2}$ and $\Gamma = 1.56 \pm 0.07$) and residuals of the fit. Right panel: 68, 90, 99% confidence contours of the redshift versus line intensity.

tion corrected 2–10 keV luminosities are $1.3 \times 10^{43} \text{ erg s}^{-1}$ and $1.1 \times 10^{44} \text{ erg s}^{-1}$ respectively. The measured values of intrinsic absorption and luminosity classify source 48 as a type 2 quasar candidate.

4.3 Average spectra as a function of redshift

The hypothesis that strong obscuration is ubiquitous among high X/O sources could be quantified once a redshift estimate is available. In the CDFS, after a careful check of the optical X-ray associations which were found to be discrepant between the published X-ray and optical catalogues (Giacconi et al. 2002; Alexander et al. 2003; Szokoly et al. 2004; Zheng et al. 2004), we have considered

in addition to the 15 spectroscopic redshifts, 28 photo-z. Most of them (25) have been selected from the Zheng et al. (2004) compilation requiring a quality flag ≥ 0.5 ⁵, two from the COMBO-17 survey (Wolf et al. 2004) and for one further object, though the photo-z quality flag is 0.3, the detection of an iron line at the same redshift (Gilli, private communication) makes us confident on the redshift estimate. Five sources satisfying the quality flag criterion have been excluded due to the extremely large errors quoted by Zheng et al. (2004). In the CDFN we consider all the available redshifts, 5 spec-

⁵ A quality flag 0.5 means that two independent codes (the BPZ–Bayesian Photometric Redshift estimation, Benitez 2000; HyperZ, Bolzonella et al. 2000) return consistent values.

Table 4. Redshift values for each redshift bin: in col. 1 the mean redshift weighted by the counts of the sources in each bin, in col. 2 and 3 the maximum and minimum redshift of the sources in each bin.

	mean z	min z	max z
CDFS	0.80	0.36	0.99
	1.15	1.016	1.32
	1.68	1.51	1.99
	2.46	2.19	2.942
	3.12	3.064	3.66
CDFN	0.49	0.474	0.52
	1.09	0.986	1.146
	1.46	1.25	1.609
	2.27	1.93	2.52

Table 5. Spectral fit parameters of the spectra in redshift bins obtained with a power law model plus intrinsic absorption at the mean redshift (the two entries for each bin correspond to a fit with Γ free to vary and to a fit with $\Gamma=1.8$).

	z^a	number of sources	Γ	N_H^b (1)	$\chi^2/\text{d.o.f.}$
CDFS	0.80	9	1.29 ± 0.09	$0.44^{+0.31}_{-0.24}$	117.0/111
			1.8	1.32 ± 0.23	144.0/112
	1.15	6	$0.90^{+0.08}_{-0.11}$	$2.56^{+1.19}_{-1.11}$	76.7/74
			1.8	8.39 ± 0.8	147.1/75
	1.68	12	1.41 ± 0.06	$1.51^{+0.58}_{-0.48}$	184.7/161
			1.8	$3.29^{+0.41}_{-0.39}$	218.3/162
	2.46	12	$1.35^{+0.11}_{-0.13}$	$12.98^{+3.23}_{-2.52}$	97.1/102
			1.8	$19.98^{+2.51}_{-2.26}$	114.1/103
	3.12	4	$1.20^{+0.12}_{-0.14}$	$8.86^{+4.93}_{-3.57}$	44.6/50
			1.8	$20.62^{+4.20}_{-3.65}$	65.0/51
CDFN	0.49	3	1.23 ± 0.12	$1.39^{+0.48}_{-0.26}$	83.6/80
			1.8	$2.48^{+0.28}_{-0.26}$	103.4/81
	1.09	4	1.18 ± 0.06	$2.74^{+0.43}_{-0.34}$	286.6/190 ^c
			1.8	5.54 ± 0.36	403.4/191 ^c
	1.46	6	1.58 ± 0.05	$5.62^{+0.60}_{-0.50}$	278.7/215
			1.8	$6.92^{+0.38}_{-0.39}$	295.9/216
	2.27	6	0.98 ± 0.15	$4.32^{+2.75}_{-2.00}$	72.6/63
			1.8	$12.91^{+3.06}_{-2.55}$	104.9/64

^a Mean value weighted by the counts of the sources in each bin. ^b Units of 10^{22} cm^{-2} .

^c The statistical quality of the fit is bad due to the presence of a strong Fe $K\alpha$ iron line at E=2.9 keV (Comastri, Brusa & Civano 2004) and to another iron line at E \simeq 3.0 keV.

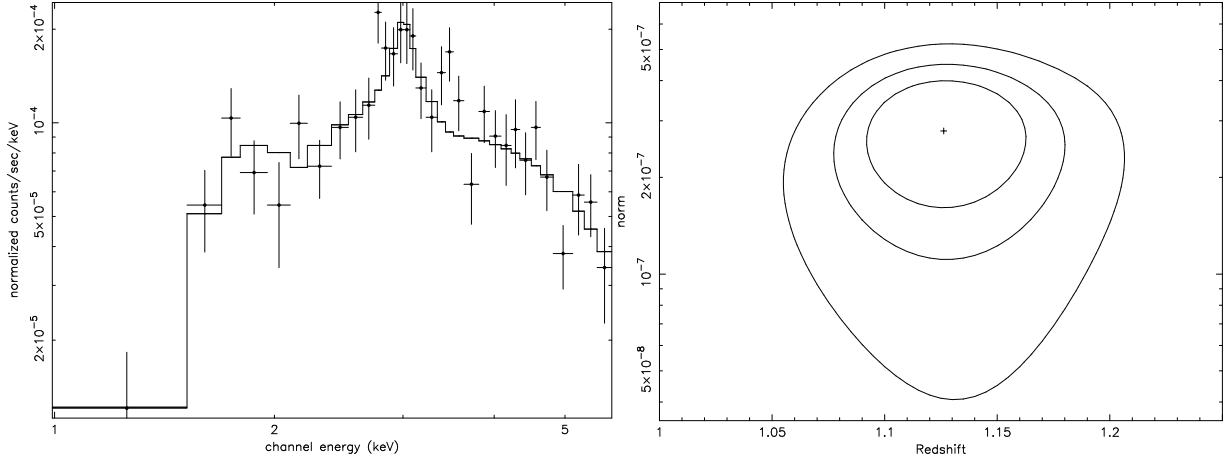


Figure 7. Left panel: the X-ray spectrum of source 48 (CDFN), fitted with an absorbed power-law plus a FeK α line (the best-fit column density and spectral slope are $N_H = 3.2 \pm 0.3 \times 10^{23} \text{ cm}^{-2}$ and $\Gamma = 1.88 \pm 0.07$). Right panel: 68, 90, 99% confidence contours of the redshift versus the line intensity.

troscopic plus 12 reliable photo- z (according to Barger et al. 2003) computed with the BPZ code. Not surprisingly, the sources without a redshift measurement are, on average, optically fainter (most of them with $R > 25$). For two sources in the CDFN a reliable redshift estimate has been obtained directly from the X-ray data thanks to the detection of a K α line (see Sect. 4.2).

All the redshifts considered for the spectral analysis are reported in column 8 of Table 1 and in column 7 of Table 2, along with a flag in column 9 and 8, respectively (phot = photometric, spec = spectroscopic, K α = iron line).

The 62 sources with spectroscopic (20), photometric (40) and X-ray (2) redshift were subdivided in 9 redshift bins, 5 for CDFS and 4 for CDFN (see Table 4 for details). Each bin is centered at the redshift value obtained by weighting the source counts for a given interval.

Stacked spectra of the sources in each redshift bin were extracted and fitted with a power-law model plus intrinsic absorption at the mean redshift. At first, N_H and Γ were free to vary, then the power-law slope has been fixed to $\Gamma = 1.8$ in order to better constrain the intrinsic absorption column density. The 95% confidence level errors on the photo- z of eight CDFS sources is larger than the bin width. We have verified that excluding these sources does not significantly modify the results and thus all of them were included and assigned at the redshift bin corresponding to the best fit photo- z . The best-fit N_H values are reported in Table 5, and plotted in Figure 8.

The results in both fields unambiguously confirm that high X/O sources are highly obscured with rest frame column densities larger than 10^{22} cm^{-2} . The average value of the column density at $z \simeq 3$ is of the order of $2 \times 10^{23} \text{ cm}^{-2}$. As an independent check, the individual spectra of the brightest objects, spread over the entire redshift range and with enough counts (> 200) to perform moderate-quality spectral analysis, have been fitted with a $\Gamma = 1.8$ power-law plus rest-frame absorption. In all the cases the fitted N_H is consistent with the value obtained for the stacked spectrum in the corresponding redshift bin.

A clear trend is evident in Fig. 8 suggesting an increasing of the average column density towards high redshifts. Such a correlation might well be due to a selection effect. Obscured sources at low redshift could have been missed simply because were too faint. At higher redshifts the photoelectric cut-off is moved towards lower

energies where the *Chandra* effective area is higher, favouring the detection of higher column densities.

In order to verify whether the observed trend is due to a selection effect, extensive Montecarlo simulations have been performed using the *fakeit* routine within XSPEC. A power-law spectrum with $\Gamma = 1.8$, normalized to encompass the observed range of 2–8 keV fluxes, is simulated for different values of the column density ($10^{22-23.5} \text{ cm}^{-2}$) over the redshift interval $z = 0.1-3.5$. For each redshift the maximum N_H value for which a source could be detected at the faintest flux of our sample has been computed. The results (Fig. 8) indicate that obscured sources ($N_H \sim 10^{23} \text{ cm}^{-2}$) at relatively low redshift ($z \simeq 1$) would have been detected in the deep *Chandra* field. It should be noted that the dashed curve in Fig. 8 would be shifted towards lower N_H values, if the power law slope is left free to vary in the range $\Gamma \simeq 1-1.4$. However, also the observed N_H value, with Γ free to vary, moves to lower values (see Table 5), leaving almost unchanged the bias estimated with $\Gamma = 1.8$.

As a further check, we have simulated the expected distribution of counts in the very hard 4–7 keV band for the range of column densities and redshifts considered here. The results indicate a change in the number of counts of $\sim 10-20\%$ (at most) at the highest column densities and lower redshift. Overall, this counts distribution is consistent with the one observed in the 4–7 keV energy range in the stacked spectra of different redshift bins. Although we are confident that the present findings are not strongly biased against low-redshift absorbed sources such a possibility cannot be completely ruled out. Indeed, the simulations suggest that the sensitivity limit to absorption decreases, as expected, at low redshifts. As a result, for a given column density ($N_H \geq 10^{22} \text{ cm}^{-2}$), faint sources are more easily missed if they are at lower redshift.

5 DISCUSSION

The results of spectral analysis of a large sample of high X/O sources in the *Chandra* deep fields leave no doubts about the presence of X-ray absorption. Similar results have been recently obtained for a sample of high X/O sources detected at brighter fluxes ($> 10^{-14} \text{ erg cm}^{-2} \text{ s}^{-1}$) in the HELLAS2XMM survey (Perola et al. 2004; Comastri & Fiore 2004).

The shape of the stacked spectrum in both CDFN and CDFS and the residuals with respect to a single power-law fit are consis-

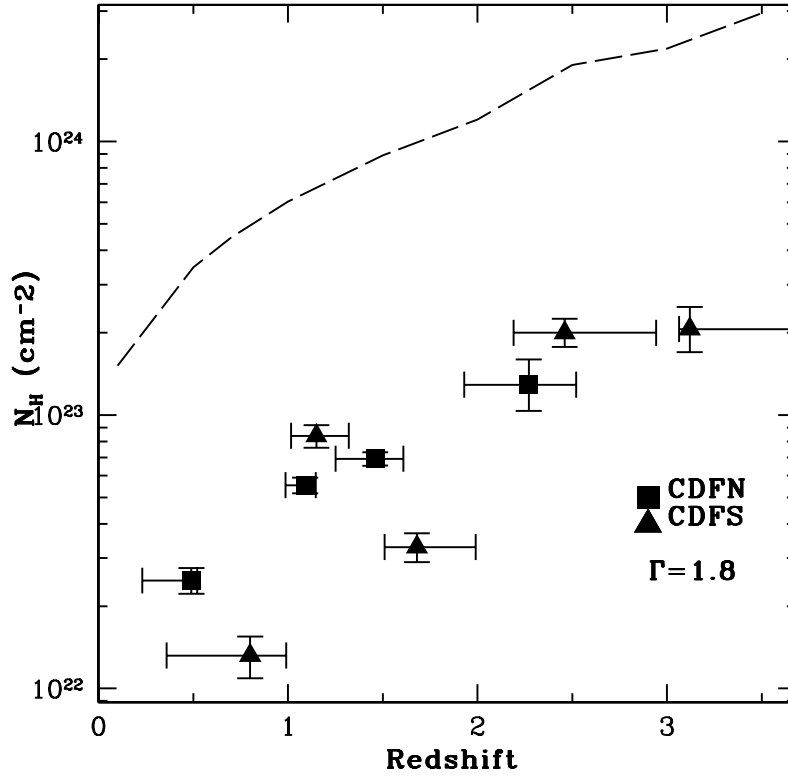


Figure 8. Intrinsic N_H rest frame distribution for the stacked spectra in different redshift bins. Symbols as in figure 4. The dashed line represents the detection limit obtained by the simulations described in Section 4.3.

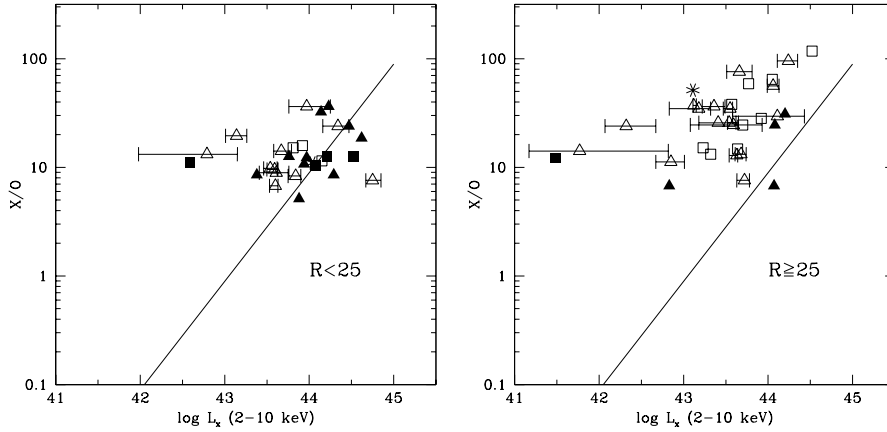


Figure 9. The X-ray to optical flux ratio as a function of the 2-10 keV deabsorbed luminosity for the 61 sources with redshift information (CDFN = squares, CDFS = triangles, filled symbols = spectroscopic redshift, open symbols = photometric redshift, stars = redshift trough iron line). The error bars corresponds to the quoted uncertainties on the photo-z. Left panel: optically "bright" sources ($R < 25$). Right panel: optically faint objects ($R \geq 25$). The extrapolation of the Fiore et al. (2003) relation is also reported (continuous line).

tent with those expected by obscured sources spread over a range of redshifts. The very hard average slope $\Gamma \simeq 0.9$ – 1.0 in the CDFS and $\Gamma \simeq 0.6$ – 0.9 in the CDFN is consistent with that obtained for a sample of hard (2–7 keV) and ultrahard (4–7 keV) selected sources ($\Gamma \simeq 1.0$ – 1.1) in the *Chandra* Groth Strip survey (Nandra et al. 2004). Surprisingly, the fraction of the high X/O sources in the *Chandra* deep fields (about 23%) is comparable to that (about

25%) of hard spectrum objects in the Groth Strip sample. The most straightforward explanation would imply that most of the hard sources in the Groth Strip survey have high X-ray to optical flux ratios. Such a possibility could be easily tested thanks to the multi-band imaging including HST/ACS observations. It is also worth noting that the average spectrum of the sources in the Groth Strip

survey has been computed with the hardness ratio technique and thus affected by larger uncertainties.

Most interesting, the average spectral shape of our sample as a function of the hard X-ray flux is approximately constant. Such a behaviour is significantly different from the well established trend observed in the same *Chandra* fields (Rosati et al. 2002; Alexander et al. 2001, 2003) without a specific selection on the X-ray to optical flux ratio. Given that fainter X-ray sources are most likely at higher redshifts, the observed shape can be explained if more distant sources are, on average, more obscured. Indeed, such a trend seems to be present for those sources (about half of the sample) for which a redshift estimate has been considered. Though potentially interesting, such a correlation needs to be confirmed by a larger sample, with a larger fraction of spectroscopic identification, allowing to keep the observational biases under control.

Unfortunately, the spectroscopic identification of obscured high X/O sources is already challenging the capabilities of large 8–10 m class telescopes. An alternative method to multiband optical/near-infrared photometry and Fe K α line X-ray spectroscopy has been put forward by Fiore et al. (2003). The X/O ratio and 2–10 keV luminosity of a large sample of spectroscopically identified hard X-ray selected sources follow a linear relation: $\log L_{2-10} = \log f(2 - 10\text{keV})/f(R) + 43.05$. The correlation holds for optically obscured sources (i.e., non broad-line AGN) and has been calibrated combining the optical and X-ray data of the HELLAS2XMM survey with well defined subsamples of identified sources in the deep *Chandra* fields at fluxes larger than $3 \times 10^{-15} \text{ erg cm}^{-2} \text{ s}^{-1}$, and optical magnitudes brighter than the $R \approx 24$ –25. Though characterized by a not-negligible dispersion (about 0.4 dex), this relation can be used to compute X-ray luminosities, and then redshifts of obscured sources, from the observed X/O value. The accuracy in the redshift estimate (“X-photo-z”; Fiore 2004) is fairly good [$\sigma(\Delta z/(1+z)) \approx 0.2$].

In order to check whether the Fiore et al. relation could be used to infer redshifts for the unidentified sources in our sample, we have plotted the X/O values and luminosities for the 61 sources⁶ in our sample with redshift information. The two panels of Fig. 9 show the unabsorbed 2–10 keV luminosity, calculated from the published 2–8 keV counts and exposure times (Alexander et al. 2003) assuming a power-law model with $\Gamma=1.8$ plus Galactic absorption, versus the X/O ratio for sources brighter and fainter of $R=25$, respectively. In each panel sources with spectroscopic, photometric and X-ray redshifts are plotted with different symbols and the Fiore et al. relation is also reported. While for the bright subsample there is a fairly good agreement, though characterized by a significant dispersion, with the correlation, at fainter magnitudes high X/O sources have lower luminosities than expected. Such a discrepancy, already noted by Bauer et al. (2004) and Barger et al. (2005), may indicate that the relative contribution of the host galaxy emission to the measured optical luminosity at $R > 24$ –25 is different than at brighter magnitudes. As a consequence some caution should be used when the Fiore et al. relation is extrapolated to optically faint objects.

The X/O vs. X-ray luminosity relation has been employed by Padovani et al. (2004) to search for type 2 quasars combining deep *Chandra* exposure with HST/ACS imaging within the GOODS project. Almost by definition a large fraction of the candidate type

2 quasars ($N_H > 10^{22} \text{ cm}^{-2}$, $L_X > 10^{44} \text{ erg s}^{-1}$) of the Padovani et al. (2004) sample have X/O > 1 . Given that most of them have faint R-band magnitudes, the high space density of type 2 quasars obtained by Padovani et al. (2004) should be considered as an upper limit.

Although the observed trend seems to indicate that the X/O vs. luminosity relation does not hold at $R > 25$, it is important to note that at faint optical magnitudes the probability to find by chance a galaxy in the X-ray error box increases dramatically (i.e. up to about 0.25–0.30 for $R=26$ and an error circle radius of 2 arc-sec, without considering source clustering). Furthermore, photo-z estimates often involve the determination of the magnitudes of the sources in images of very different quality (e.g., space versus ground based telescopes) and, as a consequence, are affected by systematic errors (see Zheng et al. 2004 for a discussion on the accuracy of redshift estimates in the CDFS).

6 CONCLUSIONS

The most important results obtained from the spectral analysis of a large sample of high X/O sources selected from deep *Chandra* fields can be summarized as follows:

- The average slope obtained by fitting the stacked spectra with a single power-law model in both CDFN and CDFS is extremely flat ($\Gamma \sim 1$). The shape of the residuals strongly suggests that such a hard slope may well be the result of the superpositions of sources with different intrinsic column densities over a broad range of redshifts.
- The average slope of the stacked spectrum is almost independent from the 2–8 keV flux. The high X/O sources represent the most obscured component of the X-ray background. Their spectra are harder ($\Gamma \lesssim 1$) than any other class of sources in the deep fields and also of the XRB spectrum.
- The redshift estimates, mainly obtained by multiband optical and near-infrared imaging, available for about half of the sample, allowed us to investigate the amount of intrinsic absorption in the stacked spectra for a few redshift ranges. A trend of increasing absorption with redshift has been uncovered ($N_H = 10^{22-23.5} \text{ cm}^{-2}$). While observational biases could not be completely ruled out, extensive simulations suggest that the observed trend may well be real. Also, the rather constant hard spectrum over more than two orders of magnitude X-ray flux is consistent with such a behaviour.
- Two new X-ray redshifts, obtained from the K α iron line, have been discovered. One object satisfy the criterion of an X-ray type 2 QSO.
- Though the X/O ratio is a fairly good estimator of the source luminosity and redshift (Fiore et al. 2003), at faint optical magnitudes ($R > 25$) a departure from the X/O vs. luminosity relation is emerging.

A large sample of high X/O sources at relatively bright X-ray fluxes will be obtained in the next few years with the COSMOS survey: a contiguous 2 square degree area observed with ACS/HST where, along with medium-deep XMM exposures, a large body of multiwavelength data is available. The full exploitation of this unique database will allow us to quantitatively estimate the redshift and absorption distribution of bright high X/O sources.

⁶ We did not include 1 broad line AGN because the Fiore et al. correlation does not hold for type 1 AGN.

7 ACKNOWLEDGMENTS

It is a pleasure to thank Piero Ranalli for help in data reduction, Fabrizio Fiore, Roberto Gilli, Guido Risaliti, Paolo Tozzi and Cristian Vignali for useful discussion. An anonymous referee is also thanked for a fast report which allow us to improve the presentation and discussion of the results. The authors acknowledge partial support by the MIUR grant COFIN-03-02-23 and by the INAF grant 270/2003.

REFERENCES

- Alexander D.M., Brandt W.N., Hornschemeier A.E., Garmire G.P., Schneider D.P., Bauer F.E., Griffiths R.E., 2001, *AJ*, 122, 2156
- Alexander D.M. et al., 2003, *AJ*, 126, 539
- Arnaud K.A., 1996, in Jacoby G., Barnes J., eds, *ASP Conf. Ser. Vol. 101, Astronomical Data Analysis Software and System V. Astron. Soc. Pac.*, San Francisco, p. 17
- Barger A.J. et al., 2003, *AJ*, 126, 632
- Barger A.J., Cowie L.L., Mushotzky R.F., Yang Y., Wang W.H., Steffen A.T., Capak P. 2005, *AJ*, in press (astro-ph/0410527)
- Bauer F.E. et al., 2002, in Done C., Puchnarewicz E.M., Ward M.Jin, eds, "New X-ray Results from Clusters of Galaxies and Black Holes", in press (astro-ph/0212389)
- Bauer F.E., Alexander D.M., Brandt W.N., Schneider D.P., Treister E., Hornschemeier A.E., Garmire G.P., 2004, *AJ*, 128, 2048
- Benítez N., 2000, *ApJ*, 536, 571
- Bertin E., Arnouts S., 1996, *A&AS*, 117, 393
- Bolzonella M., Miralles J.M., Pelló R., 2000, *A&A*, 363, 476
- Brusa M. et al., 2004, *A&A*, in press (astro-ph/0409257)
- Brusa M., 2004, PhD Thesis, Bologna University (astro-ph/0406435)
- Comastri A., Setti G., Zamorani G., Hasinger G., 1995, *A&A*, 296, 1
- Comastri A., Brusa M., Mignoli M., 2003, *AN*, 324, 28
- Comastri A., Brusa M., Civano F., 2004, *MNRAS*, 351, L9
- Comastri A., Fiore F., 2004, "Baryons on Cosmic Structures", Kluwer Academic Publisher, in press (astro-ph/0404047)
- Ferrarese L., Merritt D., 2000, *ApJ*, 539, L9
- Fiore F. et al., 2003, *A&A*, 409, 79
- Fiore F., 2004, in Maiolino R., Mujica R., eds, "Multi-wavelength AGN surveys", World Scientific, Singapore, p. 11
- Giacconi R. et al., 2002, *ApJS*, 139, 369
- Gilli R., Salvati M., Hasinger G., 2001, *A&A*, 366, 407
- Hasinger G. et al., 2001, *A&A*, 365, L45
- Maccacaro T., Gioia I.M., Wolter A., Zamorani G., Stocke J.T., 1988, *ApJ*, 362, 680
- Mignoli M. et al., 2004, *A&A*, 418, 827
- Moretti A., Campana S., Lazzati D., Tagliaferri G., 2003, *ApJ*, 588, 696
- Mushotzky R.F., Cowie L.L., Barger A.J., Arnaud K.A., 2000, *Nat*, 404, 459
- Nandra K., Pounds K.A., 1994, *MNRAS*, 268, 405
- Nandra K. et al., 2004, *MNRAS*, 356, 568
- Padovani P., Allen M.G., Rosati P., Walton N.A., 2004, *A&A*, 424, 545
- Perola G.C. et al., 2004, *A&A*, 421, 491
- Rosati P. et al., 2002, *ApJ*, 566, 667
- Setti G., Woltjer L., 1989, *A&A*, 224, L21
- Stark A.A., Gammie C.F., Wilson R.W., Bally J., Linke R.A., Heiles C., Hurwitz M., 1992, *ApJS*, 79, 77
- Szokoly G.P. et al., 2004, *ApJS*, 155, 271
- Tozzi P. et al., 2001, *ApJ*, 562, 42
- Treister E. et al., 2004, *ApJ*, 155, 271
- Vanzella E. et al., 2004, *A&A*, 423, 761
- Vikhlinin A., Markevitch M., Murray S.S., Jones C., Forman W., Van Speybroeck L., 2005, *ApJ*, in press (astro-ph/0412306)
- Williams R.E. et al., 1996, *AJ*, 112, 1335
- Wolf C. et al., 2004, *A&A*, 421, 913
- Worsley M. A., Fabian A. C., Barcons X., Mateos S., Hasinger G., Brunner H., 2004, *MNRAS*, 352, 28

Zheng W. et al., 2004, *ApJS*, 155, 73

Zombeck M.V., *Handbook of space astronomy and astrophysics*, Cambridge University Press, 1990